

Polymer Science (MSE-360)

Calorimetry

Fall Semester 2025/26

Assistant:

Filip Koldzic (LMOM, MXG 040)

filip.koldzic@epfl.ch

Introduction

The mechanical and physical properties of semi-crystalline polymers strongly depend on their microstructure, which itself is influenced by the crystallization conditions experienced by the material (crystallization rate and temperature). In order to control the crystalline structure (morphology, crystallinity) and obtain the desired properties, a study of crystallization kinetics is therefore essential. For this purpose, a large number of experimental techniques have been used, such as X-ray diffraction, dilatometry, infrared spectroscopy, light scattering, etc. Among these techniques, differential scanning calorimetry (DSC) proves to be a simple and effective tool that gives many useful information.

The polymer studied in this session is poly(ethylene terephthalate) (PET). It is one of the most commonly used polymeric materials in packaging industry, particularly in the food sector (recyclable bottles). PET bottles are manufactured by stretch-blow molding (Figure 1). They are transparent, recyclable, and exhibit good mechanical and barrier properties.

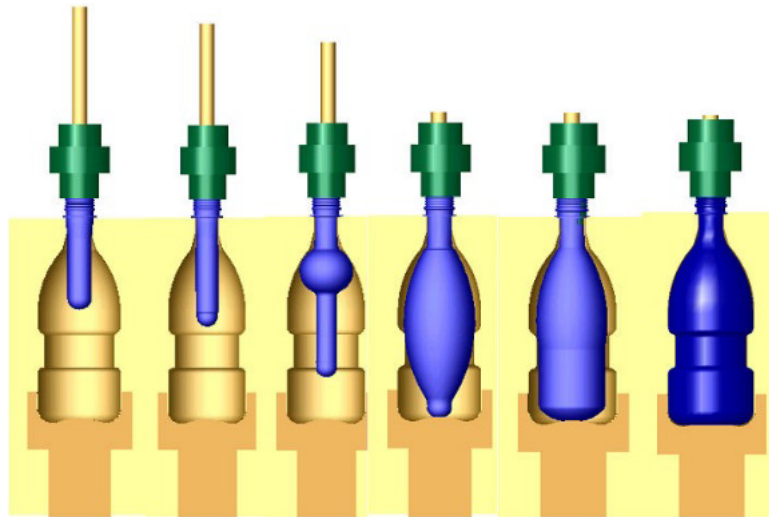


Figure 1. Schematic representation of the stretch-blow molding process of a PET bottle.

During this practical session, we will characterize the crystalline properties of PET, such as crystallization kinetics, crystallization and melting temperatures, using the technique of differential scanning calorimetry (DSC). Two types of experiments will be carried out: thermal cycles and isothermal studies. By the end of the session, you will be able to experimentally characterize the crystalline properties of a common polymer material and discuss some theoretical tools that will allow you to interpret the data you have measured.

Theoretical part

Crystallization kinetics

The Avrami model is one of the most widely used to describe the crystallization kinetics of materials. This model is semi-empirical, since the determination of its physical parameters is carried out by fitting to experimental curves. In its simplest form, the Avrami model is based on the following assumptions:

- nucleation occurs randomly and uniformly in the amorphous phase
- the growth rate does not depend on the degree of transformation

- growth is identical in all directions
- absence of secondary nucleation

The dependence of crystallinity on time $X(t)$ is then defined as follows:

$$X(t) = X_{\infty}(1 - e^{-Kt^n}) \quad (1)$$

X_{∞} is the maximum crystalline fraction reached at infinite times. K is a kinetic constant, depending on the nucleation and growth rates. n is the Avrami exponent, an integer between 1 and 4 corresponding to the sum of two terms: the first accounts for the type of nucleation (homogeneous or heterogeneous, i.e. 1 or 0), and the second corresponds to the number of crystalline growth directions (one-, two-, or three-dimensional growth, from 1 to 3).

Melting

An important parameter associated with the study of polymer crystallization is the size of the crystalline lamellae. A sufficient thickness allows the crystalline lamellae to reach a thermodynamically stable state. The melting temperature will therefore be higher the greater the lamellar thickness (Gibbs–Thomson equation).

It is common to define a thickening factor $b = L/L_0$, with L being the lamellar size just before melting and L_0 the initial lamellar size, i.e., during crystallization at the crystallization temperature T_c . The Hoffman–Weeks equation below suggests a linear relationship between the melting temperature and the crystallization temperature, depending on the thickening factor:

$$T_m = \frac{T_c}{\beta} + T_{m,\infty}(1 - \frac{1}{\beta}) \quad (2)$$

$T_{m,\infty}$ is the equilibrium melting temperature, i.e., the melting temperature of a crystal of infinite size. It is one of the most important thermodynamic parameters of polymer systems. It can be determined by extrapolating the melting temperature T_m using the Hoffman–Weeks equation.

DSC Principles

Differential Scanning Calorimetry (DSC) is a thermal analysis technique that can be used to determine phase transitions parameters: the glass transition temperature (T_g), melting (T_m), and crystallization temperatures (T_c) and corresponding enthalpies. DSC measures the differences in heat exchange between the environment (furnace) and the analyzed sample, on the one hand, and between the environment and a reference sample, on the other hand. The reference sample is generally an empty crucible. This difference in exchanges allows for precise measurement of the heat flow absorbed by the polymer sample during the various transitions.

DSC curves typically represent this heat flow, dH/dt (in W/g), as a function of the temperature applied in the chamber.

Degree of Crystallinity

From an experimental point of view, crystallinity (the mass fraction of the crystalline phase) is generally calculated from the melting curves:

$$X(t) = \frac{\Delta H_m}{\Delta H_{m,\infty}} = \frac{\int_0^t \left(\frac{dH_m}{dt}\right) dt}{\int_0^\infty \left(\frac{dH_m}{dt}\right) dt} \quad (1)$$

ΔH_m is the area under the melting peak (melting enthalpy in J/g). This quantity is proportional to the mass of crystalline fraction undergoing melting. $\Delta H_{m,\infty}$ is the melting enthalpy of a 100 % crystalline sample. dH_m/dt (in W/g) is the heat flow and corresponds to the change in energy (enthalpy) released as heat over time.

In analogy to equation (3), it is also possible to define a **relative crystallinity**, $X(t)/X_\infty$, as a function of crystallization time at a fixed temperature (i.e. during an isothermal study). In this case, the upper integral is the area under the heat flow curve associated with isothermal crystallization, while the lower integral is the value of this area when the crystallization process is assumed to be complete.

Experimental Part

Sample Preparation

1. Take a sample of the PET bottle. The sample mass should be between 5 and 15 mg.
2. Weigh the empty crucible using an analytical balance.
3. Place the sample in the crucible and close it using the tool.
4. Weigh the crucible with the sample using an analytical balance.
5. Place the crucible with the sample in the DSC furnace.

Experiments

During this exercise session, you will perform two types of experiments: **one thermal cycle** (heating-cooling-heating) and **3-4 isothermal experiments**.

- Perform a thermal cycle at the standard ramp rate of $10 \text{ }^\circ\text{C min}^{-1}$. Justify the choice of the lower and upper temperature limits of the cycle (read the reference papers in appendix).
- Based on the thermal cycles, carry out 3-4 isothermal experiments at temperatures that you consider suitable to study within the allocated time for this session.
- Using Eq. 3, construct the curves showing dependence of crystallinity on the crystallization time. Crystallinity should be normalized by assuming that 100 % crystallization is reached after $4 t_{1/2}$, where $t_{1/2}$ is the half-time of crystallization. Estimate the half-times of crystallization from the normalized crystallinity curves.
- Graphically represent the half- times of crystallization as a function of the isothermal temperature.
- Linearize the Avrami equation and plot the evolution of the linear function versus time. Then perform a linear regression to extract the values of the parameters K and n (Eq. 1).
- Plot the evolution of the melting temperature as a function of the isothermal crystallization temperature. Apply the Hoffman-Weeks equation and deduce the values of b (Eq. 2).

- Calculate the crystallinity of the samples subjected to the different isothermal experiments. Plot its evolution as a function of the isothermal crystallization temperature.

Discussion

1. Identify the different transition temperatures of PET during the thermal cycle. Discuss in particular the endothermic or exothermic nature of these transitions. Mention other experimental techniques that can be used to characterize these transitions.
2. Schematically draw and discuss how would the thermal cycles look if they were performed at ramp rates of 5 K min^{-1} and 20 K min^{-1} .
3. Comment on the evolution of the half-times of crystallization $t_{1/2}$ as a function of the isothermal temperatures. Which thermodynamic parameter limits the crystallization kinetics at high temperature?
4. Based on the literature, what are the possible characteristics of the crystallization process (nature of nucleation, number of growth directions) that can be deduced from the values of n and K within the framework of Avrami theory?
5. Comment on the evolution of the melting temperature as a function of the isothermal temperature. What does the value of b estimated via Eq. 3 suggest? Do you observe any deviation from the Hoffman–Weeks law? What can you conclude?
6. In your opinion, what is the effect of increasing the isothermal crystallization temperature on the mechanical properties of PET?
7. You will be given two PET films crystallized from the molten state at two different crystallization rates (slow and fast). What do you expect the crystallinity of these two materials to be (simply specify high or low) and why? How do you explain their degree of transparency or opacity?
8. Is the PET bottle amorphous or semi-crystalline? If semi-crystalline, how do you explain its transparent appearance?

Additional Reading

Sorrentino, L., Iannace, S., Di Maio, E., & Acierno, D. (2005). Isothermal crystallization kinetics of chainextended PET. *Journal of Polymer Science Part B: Polymer Physics*, 43(15), 1966-1972.

Lu, X. F., & Hay, J. N. (2001). Isothermal crystallization kinetics and melting behaviour of poly (ethylene terephthalate). *Polymer*, 42(23), 9423-9431.

Isothermal crystallization kinetics and melting behaviour of poly(ethylene terephthalate)

X.F. Lu, J.N. Hay*

Plastic Materials Laboratory, The School of Metallurgy and Materials, The University of Birmingham, Edgbaston, Birmingham, B15 2TT, UK

Received 23 April 2001; received in revised form 30 May 2001; accepted 2 July 2001

Abstract

Differential Scanning Calorimetry has been used to study the isothermal crystallization kinetics and melting behaviour of PET. Kinetic analysis indicated that the overall crystallization of PET involved two processes, attributed to primary and secondary crystallization. Secondary crystallization occurred consecutively with primary and both processes obey different Avrami time dependences. The primary process was that of heterogeneous nucleation and three-dimensional spherical growth that was confirmed by direct observation of spherulites by SEM. Secondary crystallization was that of one dimensional growth involving fibrillar growth between the primary lamellae of the spherulites. Accordingly primary crystallization has a stronger temperature dependence on temperature than secondary. Further analysis based on Hoffman–Lauritzen theory revealed that PET crystallization followed regime I kinetics at temperatures between 490 and 564 K. Below 490 K, regime II kinetics were operational. Multiple endotherms were observed in melting PET and attributed to the effect of crystal perfection and re-crystallization on heating from the crystallization temperature to the m.pt. Increasing the crystallization temperature and the rates of heating during melting scans minimized these effects.

Increases in yield stress, yield strain and decrease in elongation at break with crystallinity were ascribed to the strengthening effect of the crystals on the amorphous matrix, accompanied by the change in mechanism of tensile deformation from ductile yielding to craze-crack growth. © 2001 Elsevier Science Ltd. All rights reserved.

Keywords: Poly(ethylene terephthalate); Isothermal crystallization kinetics; Melting

1. Introduction

Poly(ethylene terephthalate) (PET) is a well established engineering polymer used in the manufacture of fibre, film, tape, mouldings and pressurized liquid containers. As with other semi-crystallisable polymer, the physical and mechanical properties of PET depend on its microstructure and so are determined by crystallization rate, the degree and quality of crystallinity. In order to control the rate of crystallization and the degree of crystallinity and to obtain the desired morphology and properties, a great deal of effort has been made into studying the crystallization kinetics and determining the change in material properties [1–18]. Many experimental techniques have been applied to these studies including calorimetry, dilatometry, infrared spectroscopy, X-ray diffraction, light scattering and others [19]. Differential scanning calorimetry (DSC) in particular has been very

successful in studying polymer crystallization kinetics [20–21].

Although PET has been largely studied, it has not been investigated in all aspects of crystallization behaviour, e.g. secondary crystallization, and some studies conflicted with one another [22–23]. This paper aimed to investigate the isothermal crystallization kinetics and mechanism of PET in more detail primarily by using DSC. Relevant to these aspects, the melting behaviour of PET and the effect of crystallinity on tensile properties have also been investigated.

2. Experimental

Commercial PET with a number average molecular weight of 16 kg mol^{-1} and polydispersity of 2.2 was supplied by ICI plc. in sheet form. It was dried in a vacuum oven at 100°C for 12 h before re-moulding. Disc specimens, 3.0 mm in diameter and 1.5 mm in thickness were cut from the dried sheet and used for all DSC studies on melt-crystallization kinetics.

* Corresponding author. Tel.: +44-121-414-4544; fax: +44-121-414-5232.

E-mail address: j.n.hay@bham.ac.uk (J.N. Hay).

A Perkin–Elmer differential scanning calorimeter, DSC-2, interfaced to a PC computer was used to follow the variation of the rate of heat evolution with time. The temperature scale of the DSC was calibrated from the melting point of high purity metals (99.999%): lead (600.65 K); tin (505.06 K); indium (429.78 K); stearic acid (343.15 K). The power response of the calorimeter was calibrated from the enthalpy of fusion of indium [24], taken to be 28.47 J g^{-1} . Samples were weighted and enclosed in aluminum pans and an empty aluminum pan was used as reference.

All crystallization rate studies were carried out on completely amorphous samples. Corresponding to the different routes to crystallization temperature the samples were heated from the glass or cooled from the melt, isothermal crystallization was referred to as cold- and hot-crystallization, respectively. Isothermal cold-crystallization studies were carried out in the temperature range of 390–410 K. The samples were placed in DSC at 320 K and heated to the desired temperature at 160 K min^{-1} . They were kept at the crystallization temperature for sufficient time that the DSC trace returned to the calorimeter baseline. Isothermal hot-crystallization experiments were performed in the temperature range 480–500 K. For experiments carried out on molten materials, the samples were cooled from above the observed melting point at a rate of 160 K min^{-1} to the crystallization temperature and kept at that temperature until the DSC trace returned to the calorimeter baseline. Each result is an average of three.

A potassium hydroxide solution in methanol was used to etch the surface of crystallized PET. The morphology of the etched specimens was examined on a Jeol, model 5410, scanning electron microscope (SEM).

Tensile load-extension experiments were carried out using an Instron floor standing tester, model TT-BM. Dumbbell shaped samples were cut from compression-moulded plaques. The specimens had a gauge length of 25 mm, width 4 mm and thickness 0.8 mm. The cross-head speed was 0.01 cm min^{-1} min with an accuracy of $\pm 1\%$. The tests were conducted in a constant room at $295 \pm 1 \text{ K}$ and constant humidity of $50 \pm 1\%$. The applied loads were calibrated by standard weight and an interfaced PC computer recorded the response of samples to the applied load.

3. Results and discussions

3.1. The crystallization of PET

The isothermal crystallization exotherms of PET, obtained as described above, are shown in Figs. 1 and 2. The weight fraction crystallinity, X_t , was obtained from the ratio of the area of the endotherm upto time t divided by the

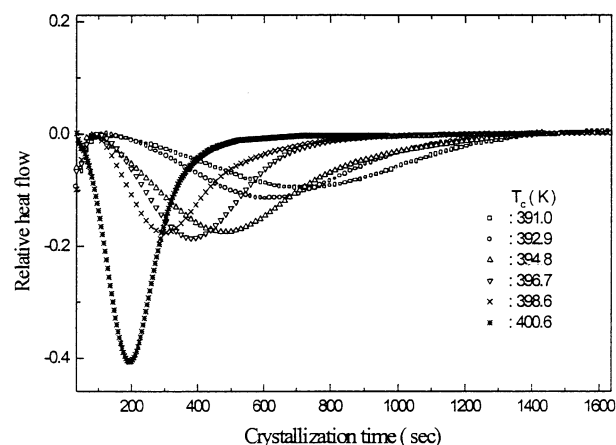


Fig. 1. DSC exotherms of the isothermal cold-crystallization of PET.

total endotherm, i.e.

$$X_t = \frac{\int_0^t (dH/dt) dt}{\int_0^\infty (dH/dt) dt} \quad (1)$$

where dH/dt is the heat flow rate. The development of the weight fraction crystallinity with time for cold- and hot-crystallization of PET is shown in Figs. 3 and 4. All isotherms exhibited a sigmoid dependence with time. The dependence of the overall crystallization rate on temperature can be seen from the half-lives in Fig. 5. The dependence of the overall crystallization rate on temperature can be seen from the variation in the half-lives in Fig. 5. This followed the conventional bell-shaped curve with the fastest rate of crystallization in the region of 430–450 K.

A slow increase of crystallinity with time after most of the crystallization had taken place was observed and this was attributed to the presence of secondary crystallization [21,25]. The time dependence was analysed assuming the presence of two crystallization processes, primary and secondary, and using a modified Avrami equation [26] for

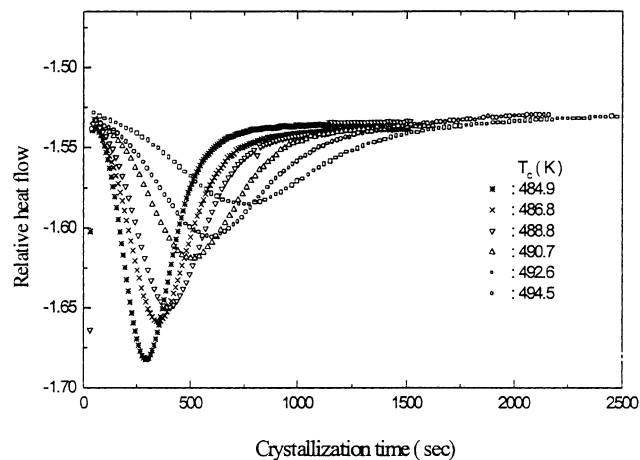


Fig. 2. DSC exotherms of the isothermal hot-crystallization of PET.

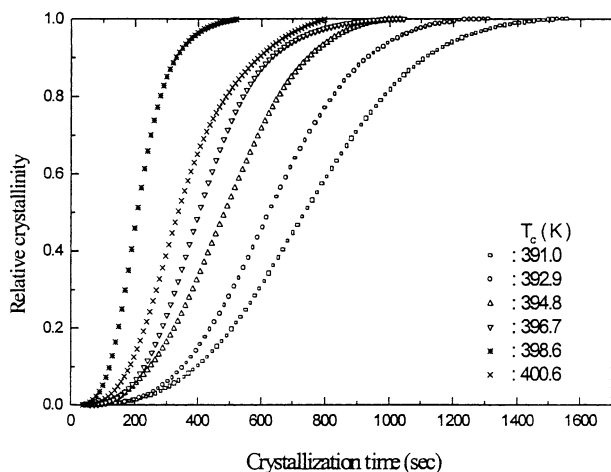


Fig. 3. Development of crystallinity with time during cold-crystallization.

which

$$X_t = X_{p,\infty} [1 - \exp(-Zt^n)] \quad (2)$$

where X_t and $X_{p,\infty}$ are the fractional extent of crystallinity at time t , and at the end of the primary process. Z is the primary composite rate constant and n a constant whose value varies according to the primary crystallization mechanism.

Eq. (2) can be differentiated and rearranged to give the n value for the primary process,

$$n = -t \left(\frac{dX_t}{dt} \right) / \left[(X_{p,\infty} - X_t) \ln \left(1 - \frac{X_t}{X_{p,\infty}} \right) \right] \quad (3)$$

Eq. (3) reflects instantaneous values of n as a function of crystallinity, X_t . Empirically, the primary and secondary crystallization processes have been considered to occur either consecutively or concurrently but the n value will predict the change from primary to secondary [26,27]. The resolution of the two processes becomes that of determining a critical value of $X_{p,\infty}$ which marks the completion of the primary crystallization. This was achieved by adjust-

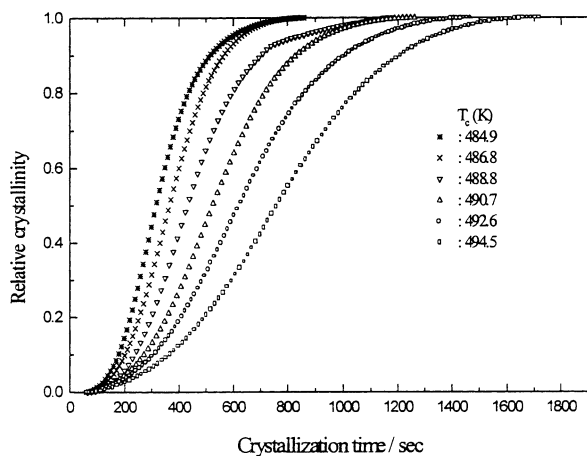


Fig. 4. Development of crystallinity with time during hot-crystallization.

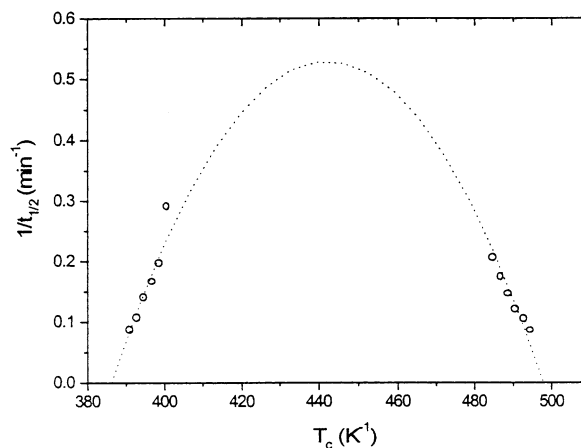


Fig. 5. The overall crystallization rate of PET as a function of crystallization temperature.

ing $X_{p,\infty}$ until the value of n remains essentially constant at the end of the primary process.

Instantaneous variation in n value with extent of crystallinity is shown typically in Fig. 6. It can be seen that the Avrami exponent changed progressively from 0.5 to 2.6 during the initial development of crystallinity, but remained at 2.6 ± 0.2 over the range 30–90% of the process. Beyond 90%, it suddenly rose towards 4.0 implying the mechanism of crystallization changed beyond the transition point corresponding to the end of the primary process, i.e. at $X_{p,\infty}$. The values of $X_{p,\infty}$ for cold- and hot-crystallization at different temperatures were obtained in this manner and are shown in Table 1.

For cold-crystallization, $X_{p,\infty}$ decreased with increase in temperature, and at the same time the rate constant of primary crystallization increased. For the hot-crystallization of PET, $X_{p,\infty}$ increased with the increasing temperature, and the rate constant of primary crystallization decreased. It would appear that a faster primary crystallization process was accompanied with an increase in the amount of secondary crystallization present.

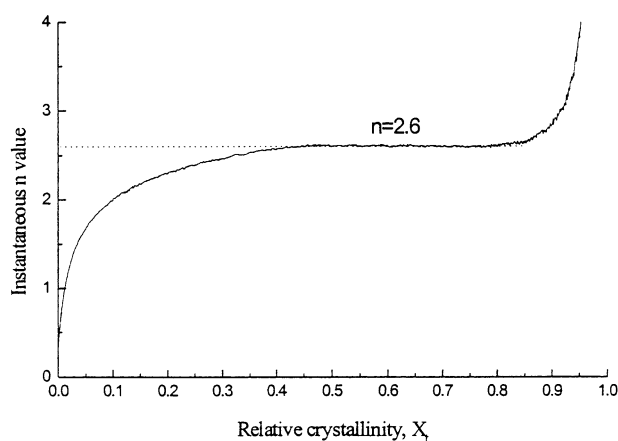


Fig. 6. Variation in n value during PET isothermal crystallization.

Table 1
 $X_{p,\infty}$ for PET isothermal crystallization

Cold-crystallization		Hot-crystallization	
Temperature (K)	$X_{p,\infty}$	Temperature (K)	$X_{p,\infty}$
391.0	0.98	484.9	0.91
392.9	0.97	486.8	0.95
394.8	0.96	488.8	0.92
396.7	0.93	490.7	0.95
398.6	0.95	492.6	0.96
400.6	0.91	494.5	0.97

3.2. Primary crystallization

The Avrami kinetic analysis of the primary crystallization process is shown in Figs. 7 and 8 for cold- and hot-crystallization respectively. A series of straight lines were obtained from plots of $(-\ln(1 - [X_t/X_\infty]))$ against $\ln(t)$ for which the slope is equal to the Avrami exponent, n_1 and the intercept at $\ln(t) = 0$ is $\ln(Z_1)$. Values of n_1 , Z_1 and the corresponding half-life, $t_{1/2,1}$ for cold- and hot-crystallization are listed in Tables 2 and 3, respectively.

It can be seen from Tables 2 and 3 that the n values were essentially constant at 2.6 ± 0.2 for both cold- and hot-crystallization and are not the integer values required by the crystallization mechanisms considered by Avrami. The values are consistent with other polymer crystallization kinetic studies for which the mechanism is one of growth of spherulites from heterogenous nuclei. Indeed, a spherulitic morphology was observed by SEM in these crystalline samples after etching with methanolic KOH, see Fig. 9.

3.3. Secondary crystallization

Many research workers [28–30] have attributed the deviation to the presence of a secondary process. However, up to now, the exact mechanism of the secondary crystallization has not been clear, thus the analysis of secondary crystallization has been based on certain approximations.

Following Hillier's two-stage crystallization of spheru-

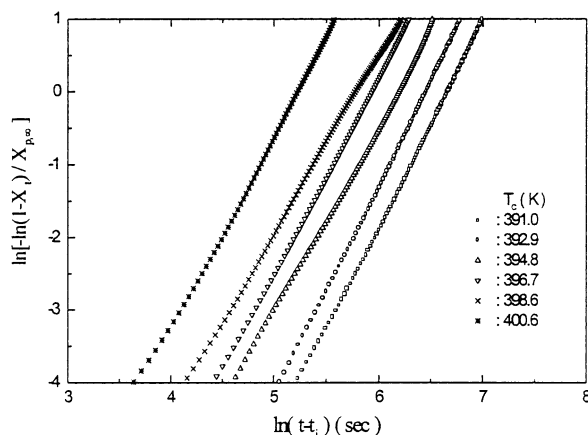


Fig. 7. Avrami analysis for the primary stage of cold-crystallization of PET.

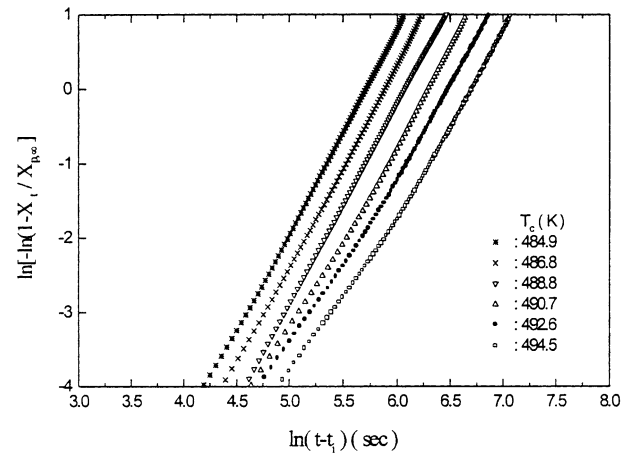


Fig. 8. Avrami analysis for the primary stage of hot-crystallization of PET.

lites in which secondary crystallization develops within the boundaries of the spherulite, Verhoyen and coworkers [31] consider that the secondary crystallization occurs well after the primary has stopped and the two follow their own Avrami kinetic equation.

Thus for the primary crystallization,

$$X_p = w_1 [1 - e^{-Z_1(t-t_{0,1})^{n_1}}] \quad (4)$$

where $t_{0,1}$ is an induction time for the primary crystallization, and Z_1 and n_1 represent the Avrami constant and rate constant, respectively.

For the secondary crystallization,

$$X_s = w_2 [1 - e^{-Z_2(t-t_{0,2})^{n_2}}] \quad (5)$$

where $t_{0,2}$ is the induction time for the secondary crystallization. The essential and necessary condition for the model is $t_{0,2} \gg t_{0,1}$. n_2 and Z_2 represent the Avrami constant and rate constant of the secondary process, respectively. w_1 and w_2 represent the relative importance of the two processes and $w_1 + w_2 = 1$. The total crystallinity developing with time is thus given by

$$X_t = w_1 [1 - e^{-Z_1(t-t_{0,1})^{n_1}}] + w_2 [1 - e^{-Z_2(t-t_{0,2})^{n_2}}] \quad (6)$$

This equation was used to analyse the crystallization of PET in this study. The relative importance of the two processes, w_1 and w_2 , is reflected by the relative degree of crystallinity at the end of primary crystallization, $X_{p,\infty}$, and the secondary process, $X_{s,\infty}$, respectively. An additional assumption was made that the secondary process started at the end of the primary process. Thus, $t_{0,2}$ was set as the time

Table 2
 The Avrami rate parameters for PET (Primary stage of cold-crystallization)

T_c (K)	391.0	392.9	394.8	396.7	398.6	400.6
$n_1 \pm 0.1$	2.6	2.5	2.6	2.7	2.6	2.5
$Z_1 \times 10^3$ (min^{-n_1})	1.24	2.66	5.19	7.24	18.6	68.0
$t_{1/2,1}$ (min)	11.4	9.26	6.57	5.42	4.25	3.45

Table 3
Avrami rate parameters for PET (Primary stage of hot-crystallization)

T_c (K)	484.9	486.8	488.8	490.7	492.6	494.5
$n_1 \pm 0.1$	2.7	2.7	2.7	2.5	2.4	2.4
$Z_1 \times 10^3$ (min $^{-n_1}$)	12.6	7.99	4.75	4.20	3.49	2.71
$t_{1/2,1}$ (min)	4.41	5.22	6.33	7.71	8.72	10.1

when the primary process finished and the secondary process started.

The total crystallinity at time, t , has two time dependences, i.e. initially when, $X_t < X_{p,\infty}$,

$$X_t = X_p = X_{p,\infty} [1 - e^{-Z_1(t-t_{0,1})^{n_1}}] \quad (7)$$

and when, $X_t > X_{p,\infty}$,

$$X_t = X_{p,\infty} + X_s = X_{p,\infty} + X_{s,\infty} [1 - e^{-Z_2(t-t_{0,2})^{n_2}}] \quad (8)$$

The cold- and melt-crystallization rates were analysed in terms of these two regions and the kinetic parameters of the secondary crystallization, i.e. the Avrami constant, n_2 , rate constant, Z_2 , and the half-life, $t_{1/2}$, obtained. These are listed in Tables 4 and 5, respectively.

From Tables 4 and 5 it can be seen that the n_2 values were about 1.2, suggesting that one dimensional crystal growth is occurring in the final stage of the crystallization. The values of Z_2 and $t_{1/2}$ are dependent on temperature and changing in the same relative way as the values for primary crystallization. In the temperature region of cold-crystallization, the rate of the secondary process decreased with decreasing temperature consistent with the increase in melt viscosity as the glass transition is approached. In the temperature region of hot-crystallization, the rate constant decreased with increasing temperature consistent with nucleation control of crystallization.

Secondary crystallization develops after 90% of the crystallization process has taken place and the kinetic analysis is severely restricted by the limited sensitivity of the DSC. Secondary crystallization continues to develop well beyond

Table 4
Avrami rate parameters for PET (Secondary process of cold-crystallization)

T_c (K)	391.0	392.9	394.8	396.7	398.6	400.6
$n_2 \pm 0.1$	1.3	1.3	1.2	1.2	1.2	1.2
Z_2 (min $^{-n_2}$)	0.17	0.25	0.28	0.32	0.39	0.48
$t_{1/2,2}$ (min)	4.1	3.3	2.5	2.2	1.8	1.5

the detectable limit of heat flow measurements in the DSC and this reduces the accuracy of determining the rate constants and n value.

3.4. Nucleation characteristics

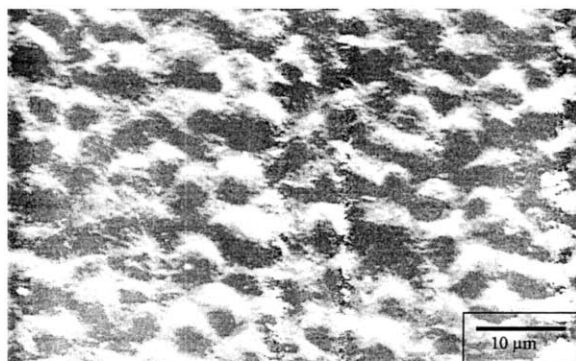
The crystallization characteristics of thin films of PET were studied by hot stage microscopy. Resolvable spherulites were observed in the temperature range 110 to 160°C. The radii of the spherulites were observed to grow linearly with time up to impingement and the nucleation density was measured from the number of spherulites in the field of view. Radial growth rates increased and nucleation densities decreased with crystallization temperature in the range of cold-crystallization, as can be seen in Fig. 10. Nucleation was heterogeneous as the spherulites reformed in same place within the PET sample on melting and crystallization. Heterogeneous nuclei are most likely to form on a range of different size particles with progressively smaller ones becoming effective with decreasing temperature. The density of nuclei should increase with decreasing crystallization as the more numerous small particles become activated.

3.5. Melting and the equilibrium melting point

In order to understand the temperature dependence of the crystallization rates it was important to measure the equilibrium melting temperature of PET by establishing the rate dependence on the degree of super-cooling, $\Delta T = T_m - T_c$. As described above, PET can be crystallized over a wide temperature range between the glass transition and the melting point. The different thermal history leads to different morphologies as evidenced by the presence of multiple melting endotherms [32–35]. A weak dependence of melting point on crystallization temperature is then observed as a result of melting and re-crystallization or annealing of the sample during the heating to the melting point. This produces further structural changes within the sample. In investigating the effect of heating rate on this recrystallization and subsequent changes in melting behaviour, PET was

Table 5
Avrami rate parameters for PET (Secondary process of hot-crystallization)

T_c (K)	484.9	486.8	488.8	490.7	492.6	494.5
$n_2 \pm 0.1$	1.2	1.3	1.2	1.0	1.3	1.3
Z_2 (min $^{-n_2}$)	0.28	0.24	0.22	0.18	0.16	0.15
$t_{1/2,2}$ (min)	2.4	2.8	3.2	3.8	4.3	4.7



(10 kV x 2,000)

Fig. 9. Spherulites of PET after crystallization at 120°C for 1 h and KOH etching.

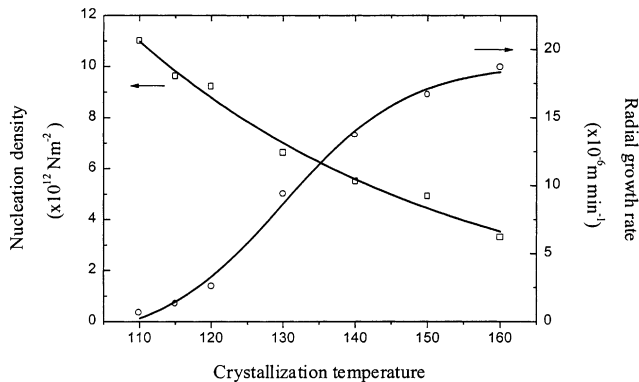


Fig. 10. Changes in nucleation density and crystal growth rate with temperature.

isothermally hot crystallized at 485 K for various periods up to complete crystallization. The samples were then melted at different heating rates from 5.0 to 20 K min⁻¹. Three melting endotherms were observed in these samples, as shown in Fig. 11, labelled 1, 2 and 3 with increasing temperature. Endotherm 1 started about 10 K above the crystallization temperature but shifted to increasing temperature with heating rate. If this is due to the melting of the smallest lamellae produced by secondary crystallization and to inter-lamellar growth it should not develop until after the primary stage is complete.

Endotherm 2 was independent of the heating rate and considered to be characteristic of the melting of the crystals formed in the primary crystallization. Endotherm 3 resulted from the melting and recrystallization of endotherms 1 and 2. Accordingly it increased in intensity with the slower heating rates with the greater amount of time for melting and re-crystallization. Increasing the rate of heating during melting minimized the effect of re-crystallization and, for a specific heating rate, re-crystallization is reduced by crystallizing the sample at higher temperatures. Reliable measurement of melting point should only be made by using high crystallization temperatures and rapid melting rates.

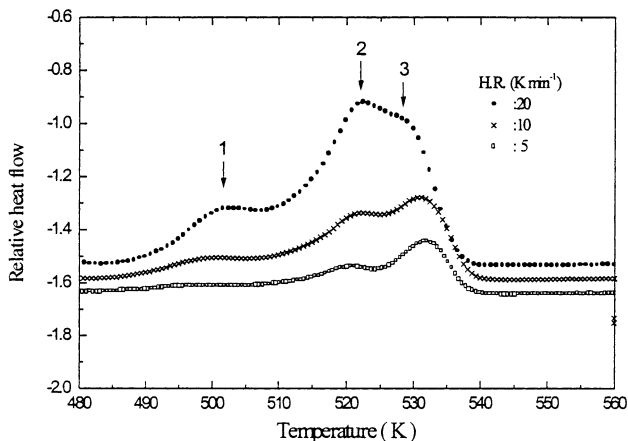


Fig. 11. Effect of heating rate on PET melting behaviour.

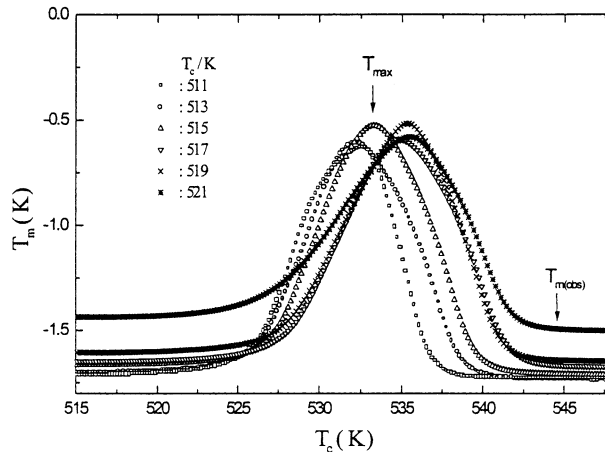


Fig. 12. The development of the melting point on crystallization temperature of PET.

Conventionally the melting point as measured by DSC is defined as the temperature corresponding to the maximum rate of melting, T_{max} . Instead, the temperature corresponding to the last trace of crystallinity of the sample [36] was adopted as $T_{m(obs)}$. Fig. 12 shows the melting endotherms at a heating rate of 20 K min⁻¹ of PET isothermal crystallization from 511 to 521 K for 24 h. Further annealing of the samples showed that a stable crystal structure had formed and the observed melting points, $T_{m(obs)}$ did not increase with further increasing time, suggesting that crystal perfection did not occur to any appreciable extent. In addition, a single melting endotherm only was observed and it shifted to higher melting points with the increasing crystallization temperature. The observed melting points were characteristic of the large stable crystals produced at the crystallization temperature.

Using these values, corrected for thermal lag, the procedure suggested by Hoffman et al. [37] was adopted of plotting $T_{m(obs)}$, against T_c to determine the equilibrium melting point, T_m^0 . The plot was linear, see Fig. 13, and could be interpolated to intersect the line of $T_m = T_c$ at a value for T_m^0

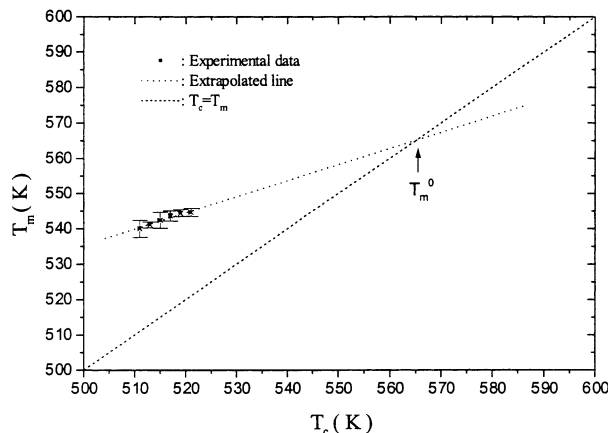


Fig. 13. The determination of the equilibrium melting point.

of 564.0 ± 2.0 K. The slope of the line, i.e. $1/2\beta$ was equal to 0.50 ± 0.1 , giving $\beta = 1.0$. This confirmed that no crystal perfection and recrystallization had occurred and caused the thickness of lamellae to increase as PET was further annealed, or while it was being heated during the melting run.

3.6. The temperature dependence of primary and secondary crystallization rates

The primary and secondary crystallization rates at different temperatures were expressed in the form of reciprocal crystallization half-life, $1/t_{1/2}$, using Hoffman–Lauritzen relationship [38] and following Chan and Isayev [39], $(1/t_{1/2})$ and $(1/t_{1/2})_0$ were used to substitute for g and g_0 , respectively. The temperature dependence of the crystallization half life ($1/t_{1/2}$) is given by

$$\left(\frac{1}{t_{1/2}}\right) = \left(\frac{1}{t_{1/2}}\right)_0 \exp\left[\frac{-U^*}{R(T - T_\infty)}\right] \exp\left[\frac{-K_g}{T(\Delta T)f}\right] \quad (9)$$

Plots of $\ln[(1/t_{1/2}) + U^*/R(T - T_\infty)]$ against $1/(T\Delta T f)$ are shown in Fig. 14 for both primary and secondary crystallization. The data is consistent with two linear relationships for both primary and secondary processes, corresponding to two nucleation regimes,

It is considered that at high crystallization temperatures, corresponding to small degrees of super-cooling, regime I kinetics are operative. In this case, surface nucleation involved in crystal growth leads to rapid completion over the surface of the new phase prior to the next nucleation event. Therefore, secondary nucleation dominates crystal growth and for primary and secondary crystallization,

$$K_{g,I} = \frac{4b\sigma\sigma_e T_m^0}{\Delta H_f k} = 5.0 \times 10^5 \text{ K}^2$$

At large degrees of super-cooling, i.e. below 490 K, regime II kinetics are operative, where the rates of the secondary nucleation and the spread of the molecular strip along the growing face are comparable.

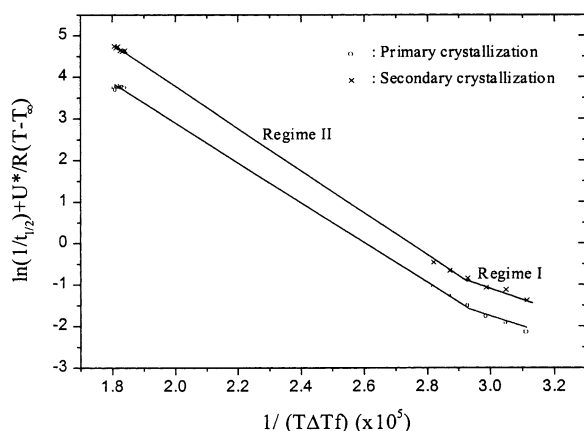


Fig. 14. $[\ln[(1/t_{1/2}) + U^*/R(T - T_\infty)]]$ versus $1/(T\Delta T f)$.

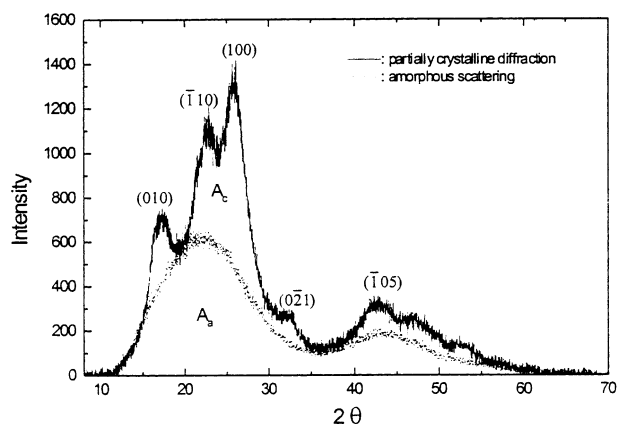


Fig. 15. WAXD diffractograms of 30% crystallized and amorphous PET.

Studies with polyethylene [38,40] also clearly show a defined transition from regime I to II accompanied by a morphology change from axialites to spherulites. PET also exhibits spherulite morphology at low temperature consistent with the regime II kinetics, applicable to PET crystallization at large super-cooling. In this case, the primary and secondary processes have the same K_g value, i.e.

$$K_{g,I} = \frac{2b\sigma\sigma_e T_m^0}{\Delta H_f k} = 2.5 \times 10^5 \text{ K}^2$$

where b is the monomolecular layer thickness, taken to be the perpendicular separation of (010) planes. This is 5.53 \AA [41]. σ is the side surface free energy of the polymer crystal, which is often estimated as [38,40,42],

$$\sigma = \partial\Delta H_f (a_0 b_0)^{1/2} \quad (10)$$

Where ∂ was derived empirically to be 0.11 by analogy with the known behaviour of hydrocarbons [43].

The unit cell dimensions, a_0 and b_0 for PET used in the analysis are 4.57 and 5.95 \AA , respectively [44]. Accordingly, for PET isothermal crystallization, $\sigma = 1.09 \times 10^{-2} \text{ J m}^{-2}$ Using $T_m^0 = 564 \pm 2 \text{ K}$ and the recommended

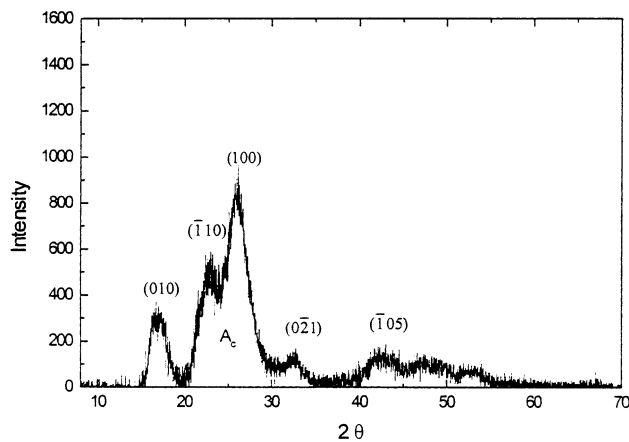


Fig. 16. The crystalline diffractogram of 30% crystallized PET after subtraction of the amorphous background.

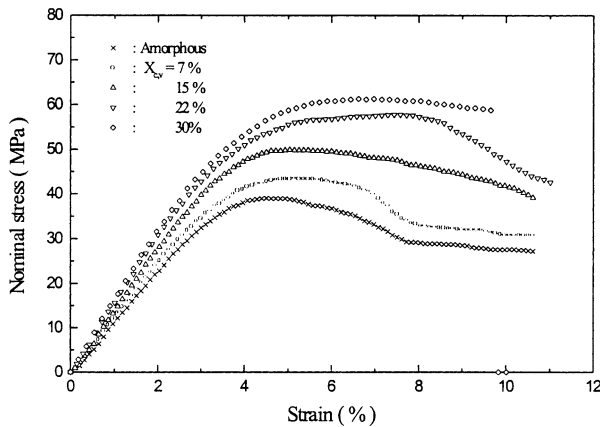


Fig. 17. The stress–strain curves of PET with various degree of crystallinity.

values [38] $U^* = 6284 \text{ J mol}^{-1}$ and [5] $\Delta H_f = 2.1 \times 10^8 \text{ J m}^{-3}$ the value of σ_e was obtained as $\sigma_e = 0.106 \pm 0.02 \text{ J m}^{-2}$. An alternative method for determining the fold surface free energy, σ_e has been applied by Wlochowicz and Przygocki [45], from small-angle X-ray diffraction to measure the fold period in PET crystal at known melting points. According to the kinetic theory of chain folding [38] they calculated σ_e for PET crystallized in temperature range 427–473 K to be $90.9\text{--}93.6 \times 10^{-3} \text{ J m}^{-2}$.

Obviously, the values for σ_e obtained in the present study are in very close agreement with these results, although a very different method was used in their calculation.

3.7. The effect of crystallinity on the tensile properties of PET

PET was annealed at 120°C for different times to produce samples of different degrees of crystallinity and their stress–strain behaviour investigated. WAXS and DSC were used to measure the degree of crystallinity. WAXS measures the volume fraction crystallinity, $X_{c,v}$. The amorphous scattering curve was scaled according to the amorphous content, and the crystalline peaks obtained by subtraction. The ratio of

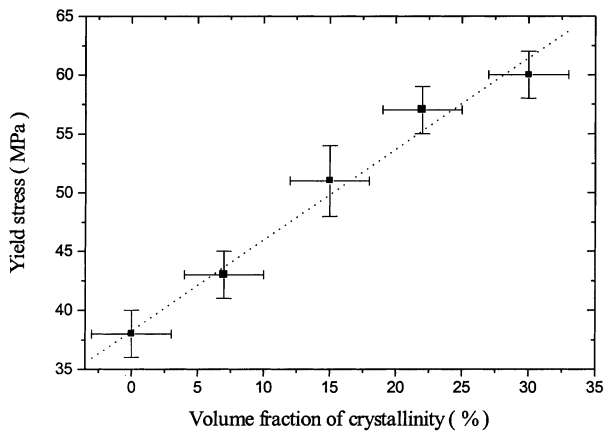


Fig. 18. The relationship between yield stress and crystallinity of PET at 23°C.

Table 6

The effect of crystallinity on the tensile properties of PET (295 ± 1 K at strain rate $4.0 \times 10^{-3} \text{ min}^{-1}$)

% Crystallinity	Yield stress (MPa)	Yield strain (%)
0	38 ± 2	3.8 ± 0.5
7 ± 3	43 ± 2	4.3 ± 0.5
15 ± 3	51 ± 3	5.3 ± 0.5
22 ± 3	57 ± 2	6.5 ± 0.5
30 ± 3	60 ± 2	7.0 ± 0.5

the area of the crystalline bands, A_c to the total area, ($A_c + A_a$), as shown in Figs. 15 and 16, was determined and used to define the volume fraction crystallinity, i.e.

$$X_{c,v} = \frac{A_c}{A_c + A_a} \quad (11)$$

These samples were subjected to stress–strain analysis as can be seen in Fig. 17. The tensile characteristics are summarized in Table 6. There was a progressive increase in the strain at yield with increasing crystallinity as well as an almost linear increase in yield stress with crystallinity, see Fig. 18. It would appear that the crystalline phase is reinforcing amorphous regions. However, as the degree of crystallinity increased shape of the neck becomes more diffuse and a region of uniform drawing eventually occurs. At this stage fracture occurs at a lower strain. Crystallization would appear to make PET more brittle as a result of increasing the yield stress and a change in fracture mechanism from ductile shear yielding to craze crack growth.

4. Conclusions

PET isothermal crystallization kinetics, including cold- and hot-crystallization were measured by using DSC. It was observed that the overall crystallization included two different steps i.e. primary and secondary crystallization, and the two occurred consecutively. The two processes were separated at a critical value of the degree of crystallinity, $X_{p,\infty}$, when there was a sudden change in the value of the Avrami exponent, n , from 2.6 to 1.2, consistent with this transition from primary to secondary.

The Avrami analysis indicated that the primary crystallization of PET followed the mechanism of three-dimension spherical growth on heterogeneous nuclei, while the secondary crystallization was linear growth within formed spherulites. The relevant kinetics parameters at various temperatures (390–400 and 480–500 K), for primary and secondary crystallizations were obtained separately.

The study on PET melting behaviour focused on the determination of the equilibrium melting point. The multiple melting peaks were ascribed to crystal perfection and recrystallization as the polymer was further annealed, or while it was being heated during the melting run. The effects of crystal perfection and recrystallization were minimized

by increasing the crystallization temperature as close as possible to the melting point temperature, and by increasing the rate of heating during the melting run. According to Hoffman and Weeks equation, the equilibrium melting point of PET, T_m^0 was determined to be 564 ± 2 K and β was 1.0 ± 0.2 . The value of β confirmed there were no further crystal perfection and recrystallization existing during the melting measurements.

Analysis using Lauritzen–Hoffman equation indicated that at temperatures above 490 K, PET crystallization followed regime I kinetics, while below 490 K, regime II kinetics was operative. The fold surface energies, σ_e for PET primary and secondary crystallizations had the same value, 0.106 ± 0.02 J m⁻², which was ten times larger than the side surface energy σ .

The increase in the yield stress, and decrease in elongation at break with degree of crystallinity was attributed to the reinforcing effect of crystalline regions on the amorphous matrix, while there was a gradual change in mechanism of tensile deformation from ductile shear yielding to craze-crack growth with the increasing crystallinity.

Acknowledgements

We would like to thank Mr Frank Biddlestone for technical support. X.F.L. acknowledges the award of an Overseas Research Student Award during the tenure of this work

References

- [1] Cobbs WH Jr, Burton RL. *J Polym Sci* 1953;X(3):275.
- [2] Keller A, Lester GR, Morgan LB. *Proc Roy Soc A* 1954;247:1.
- [3] Hartley FD, Lord FW, Morgan LB. *Proc Roy Soc A* 1954;247:2.
- [4] Van Antwerpen F, Van Krevelen DW. *J Polym Sci, Polym Phys Ed* 1972;10:2423.
- [5] Mehta A, Gaur U, Wunderlich B. *J Polym Sci, Polym Phys Ed* 1978;16:289.
- [6] Gümther B, Zachmann HG. *Polymer* 1983;24:1008.
- [7] Habarin SA. *J Appl Polym Sci* 1987;34:97.
- [8] Mayhan KG, James WJ, Bosch W. *J Appl Polym Sci* 1965;9:3605.
- [9] Mitsubishi Y, Ikeda M. *J Polym Sci, Part A2* 1966;4:283.
- [10] Ozawa T. *Polymer* 1971;12:150.
- [11] Misra A, Stein RS. *J Polym Sci, Polym Lett* 1972;10:473.
- [12] Stein RS, Misra A. *J Polym Sci, Polym Phys Ed* 1973;11:109.
- [13] South FS, Steward RD. *Polymer* 1974;15:283.
- [14] Frank WP, Zachmann HG. *Colloid Polym Sci* 1977;62:88.
- [15] Reinsch VE, Rebenfeld L. *J Appl Polym Sci* 1994;52:649.
- [16] Jackson JB, Longman GW. *Polymer* 1969;10:873.
- [17] Van Antwerpen F, Krevelen DW. *J Polym Sci, Part C* 1970;30:271.
- [18] Gunter B, Zachmann HG. *Polymer* 1983;24:1008.
- [19] Price FP. *Encycl Polym Sci Technol* 1968;8:63.
- [20] Booth A, Hay JN. *Polymer* 1969;10:95.
- [21] Hay JN, Mills PJ. *Polymer* 1982;23:1380.
- [22] Van Antwerpen F, Van Krevelen DW. *J Polym Sci, Polym Phys Ed* 1972;10:2423.
- [23] Mehta A, Gaur U, Wunderlich B. *J Polym Sci, Polym Phys Ed* 1978;16:289.
- [24] CRC handbook of chemistry and physics. 53rd ed. USA: CRC press, 1972. p. B-241.
- [25] Wunderlich B. *Macromolecular physics*, vol. 2 1976.
- [26] Hay JN. *Br Polym J* 1971;3:74.
- [27] Banks W, Gorden M, Roe R-J, Sharples A. *Polymer* 1963;4:289.
- [28] Banks W, Sharples A, Hay JN. *J Polym Sci* 1964;A-2(2):4059.
- [29] Hillier IH. *J Polym Sci, Part A* 1965;3:3067.
- [30] Price FP. *J Polym Sci, Part A* 1965;3:3079.
- [31] Verhoyen O, Dupret F, Legras R. *Polym Engng Sci* 1998;38:1594.
- [32] Bell JP, Murayama T. *J Polym Sci* 1969;A-2(7):1059.
- [33] Roberts RC. *Polym London* 1969;10:117.
- [34] Sweet GE, Bell JP. *J Polym Sci, A-2* 1972;10:1273.
- [35] Douillard A, Dumazet Ph, Chabert B, Guillet J. *Polymer* 1993;34:1702.
- [36] Flory PJ. *J Chem Phys* 1949;17:223.
- [37] Hoffman JD, Weeks JJ. *J Res Natl Bur Stand* 1962;A73:64.
- [38] Hoffman JD, Davis GT, Lauritzen JI. In: Hannay JB, editor. *Treatise on solid state chemistry: crystalline and non-crystalline solids*, vol. 3. New York: Plenum Press, 1976.
- [39] Chan TW, Isayev AI. *Polym Engng Sci* 1994;34:461.
- [40] Hoffman JD, Frolen LJ, Ross GS, Lauritzen JI. *J Res NBS* 1975;79A(6):671.
- [41] Plays LH, Phillips PJ. *J Polym Sci* 1980;18:829.
- [42] Miller RL, Boyer RF. *J Polym Sci, Polym Phys Ed* 1977;15:1475.
- [43] Daubeny R De P, Bunn CW. *Proc R Soc London A* 1954;226:531.
- [44] Turnbull D, Cormia RL. *J Chem Phys* 1961;34:820.
- [45] Wlochowicz A, Przygocki W. *J Appl Polym Sci* 1973;17:1197.

Isothermal Crystallization Kinetics of Chain-Extended PET

L. SORRENTINO,¹ S. IANNACE,² E. DI MAIO,¹ D. ACIERNO¹

¹Department of Materials and Production Engineering, University of Naples, "Federico II," Naples, Italy

²Institute of Composite and Biomedical Materials, CNR, P.le Tecchio 80, 80125 Naples, Italy

Received 16 June 2003; revised 28 February 2005; accepted 16 March 2005

DOI: 10.1002/polb.20480

Published online in Wiley InterScience (www.interscience.wiley.com).

ABSTRACT: The crystallization behavior of a commercial chain-extended PET (foam grade) was evaluated and compared to that of bottle-grade PET. Cold and melt isothermal crystallization were analyzed by using the Avrami model. The foam grade PET showed a slower crystallization kinetic compared to the bottle-grade PET. The Hoffman-Lauritzen analysis showed that the energetic barriers to nucleation and molecular mobility were higher for the chain-extended PET. This resulted in a lower nucleation rate in both cold and melt crystallization. ©2005 Wiley Periodicals, Inc. *J Polym Sci Part B: Polym Phys* 43: 1966–1972, 2005

Keywords: isothermal crystallization kinetics; barrier energy; branching

INTRODUCTION

The polymer crystallization phenomena are very important from different points of view. The molecules dimensions prevent the complete packing of chains, leaving a variable amount of amorphous phase. The presence of crystalline phase leads to materials with enhanced mechanical and gas barrier properties. Amorphous polymers are needed in those applications where it is necessary to ensure the absence of crystals for the postprocessing of intermediate manufactures (e.g., blow molding and thermoforming). It is therefore of great importance to know the crystallization kinetics to optimize the different steps of the overall process. In particular, the thermoforming process of PET is performed on amorphous sheets at temperature above T_g and close to the crystallization temperature of the materials. The optimization of the entire process can be achieved by using appropriate models able to predict the evolution of crystallinity as a function of the thermal history and temperature

profile in the sheets. Another application that requires the knowledge of the crystallization kinetics of PET is foaming. In this case, chain-extended PET are utilized because one of the critical properties for foamability is the presence of strain hardening elongational viscosity, which can be obtained by increasing the molecular weight (MW) and molecular weight distribution (MWD) of the polymer or by using branched macromolecules.^{1–3}

The crystallization kinetics of linear PET (both isothermal^{4,5} and nonisothermal^{6–8}) has been widely studied. The Avrami equation is the first (empirical) equation used to accomplish the crystallization growth. It correlates the volumetric fraction of crystalline phase $\alpha_v^c(t)$ in function of time in an isothermal process:^{9–11}

$$\alpha_v^c(t) = 1 - \exp(-kt^n) \quad (1)$$

where k is the kinetic constant, function of nucleation and growth rates, and n is the Avrami exponent, an integer from 0 to 4, which is the sum of two terms: one takes into account the nucleation type (homogeneous or heterogeneous, 1 or 0, respectively) and another the number of crystal growth directions (one-, bi-, or

Correspondence to: L. Sorrentino (E-mail: lsorrent@unina.it)

Journal of Polymer Science: Part B: Polymer Physics, Vol. 43, 1966–1972 (2005)
©2005 Wiley Periodicals, Inc.

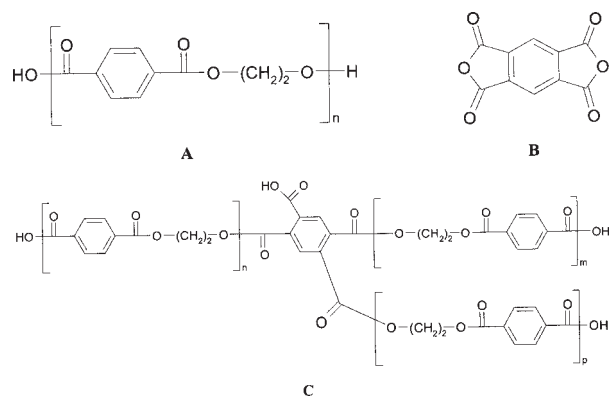


Figure 1. Structures of PET (A), PMDA (B), and a branched structure obtained by their reaction.

three-dimensional growth, from 1 to 3). This equation is in good agreement with isothermal crystallization data only for short times (depending by the crystallization temperature), due to some model simplifications such as constant polymeric phase density, constant nuclei density and crystal shape, constant radial growth rate, or no secondary crystallization. However, in addition to primary aggregation processes as in LDPE,^{12,13} secondary crystallization occurs in PET^{14–16} as well as in other common and engineering polymers.^{17–22}

For some time many efforts have been made to exceed these limits, taking into account the incomplete crystallization,^{23,24} the different phase density of amorphous and crystalline phases,^{25,26} variations of crystal growth rate,²⁷ the two different nucleation mechanisms,²⁸ and the contact of the spherulites.^{29,30}

The equation obtained by this corrections is formerly similar to eq 1, but the terms have a different meaning:

$$X_c(t) = 1 - \exp[-k(t - t_0)^n] \quad (2)$$

where $X_c(t)$ is the relative crystallinity, that is, the ratio between crystal fraction at time t and final crystal fraction, k is the kinetic constant, n is the Avrami constant, now not an integer, and t_0 is the induction time, that is, the time between the stabilization of the temperature and the time at which the crystallization starts.

In this work, the crystallization behavior of a commercial chain-extended PET with high molecular (foam grade) weight was experimentally evaluated and modeled by using the Avrami model (eq. 2). The cold and melt isothermal crystallization were analyzed by using the

theory of Hoffman-Lauritzen, which allowed the determination of the main thermodynamic properties involved in the nucleation and growth mechanism of the crystals.³¹ The results were compared to those relative to the crystallization phenomena occurring in bottle grade PET, which were taken from Lu et al.⁴

MATERIALS AND METHODS

The commercial chain extended PET (MPET) with an intrinsic viscosity of 1.25 dL/g was kindly supplied by Mossi & Ghisolfi S.p.A. The reported molecular weight distribution was characterized by a $M_w = 160,000$ with high polydispersity ($M_n = 22,000$).

Dynamic DSC scans were performed on dried samples (110 °C for 12 h in a vacuum oven) to identify the temperature ranges for isothermal tests. The samples were heated from 25 to 290 °C at 10 °C/min (I scan) and then taken at 290 °C for 4 min to cancel previous thermal history effects. The materials were then cooled to 25 °C at 10 °C/min (II scan) and then reheated again to 290 °C at 10 °C/min (III scan).

Before all the isothermal cold crystallization tests, PET samples were first melted at 290 °C for 4 min in the DSC cell to clear the previous thermal history, and then quenched in liquid nitrogen to avoid crystal nucleation. The samples were kept in anhydrous conditions before the isothermal test. For all melt crystallization experiments the samples were melted at 290 °C for 4 min and then quickly cooled at 40 °C in the DSC cell to the test temperature.

All the tests were performed in a purge flow of nitrogen to avoid the hydrolysis effects of oxygen by using a TA Instruments DSC 2920.

RESULTS AND DISCUSSION

PET molecular structure is represented in Figure 1(A). Chain extension agents are used to enhance the molecular weight, linking end groups of two macromolecular chains. The chain extender used to produce the analyzed polymer is pyromellitic dianhydride, PMDA [Fig. 1(B)], that reacts with the hydroxylic end group of two different PET macromolecules and forms two carboxylic groups. But at high temperatures these carboxylic groups can react with —OH

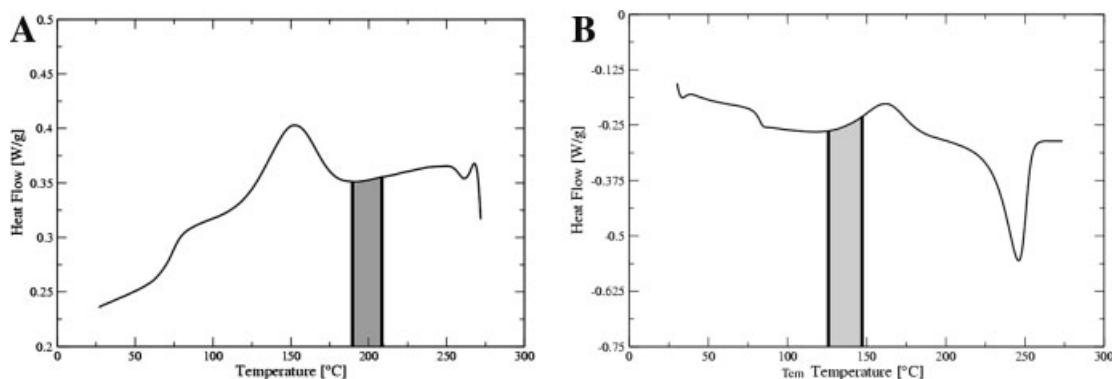


Figure 2. DSC thermograms during II scan (A) and III scan (B) at 10 °C/min.

groups leading to a branched structure and producing one H₂O molecule, as in Figure 1(C).^{32–35}

The cooling (II scan) and heating (III scan) DSC curves of chain extended PET are reported in Figure 2. As shown in Figure 2(A), MPET crystallized during the cooling scan with an exothermal peak ranging from 205 to 125 °C. The isothermal melt crystallization kinetics were investigated at temperatures ranging from 190 to 209 °C [gray area in Fig. 2(A)]. As shown in Figure 2(B), the crystallization was not complete and further crystallization occurred during the subsequent heating scan. The isothermal cold crystallization was evaluated at temperatures ranging from 125 and 145 °C [gray area in the Fig. 2(B)]. Both ranges were chosen to assure that the heat flow and the evolution of relative crystallinity could be slow enough to be precisely measured, as verified by curves in Figures 3 and 4 for the cold crystallization and Figures 5 and 6 for the melt crystallization.

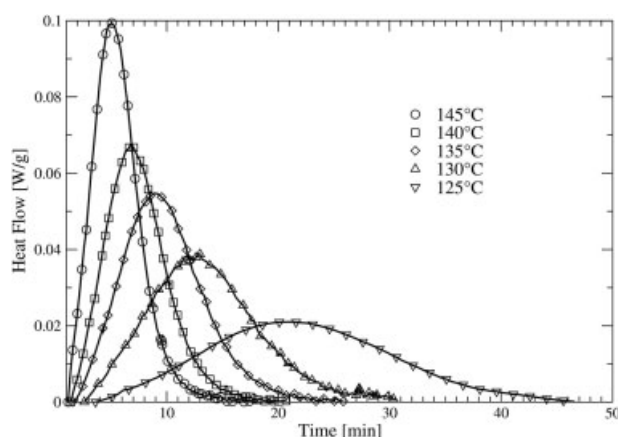


Figure 3. Heat flows versus time of low-temperature isotherms, between 125 and 145 °C.

Using the heat flow data, the relative crystallinity was evaluated using eq 3:

$$X_{C,rel}(t) = \Delta H(t) / \Delta H_{TOT} \quad (3)$$

where $\Delta H(t)$ is the heat of crystallization at time t , and ΔH_{TOT} is the total heat of crystallization. In the cold crystallization temperature range, the high undercooling of polymer melt leads to a high nucleation rate, but the overall crystallization process is hindered by the low chain folding mobility. The increase of temperature leads to a faster crystallization rate (Figs. 3 and 4) due to the increase of macromolecular mobility. As expected, an opposite behavior was observed in the melt crystallization temperature range (Fig. 5 and 6). At a temperature near the melting temperature, the molecular mobility is very high, but the limiting phenomenon is now the low nucleation rate because of the low undercooling. In this case, an increase of temperature

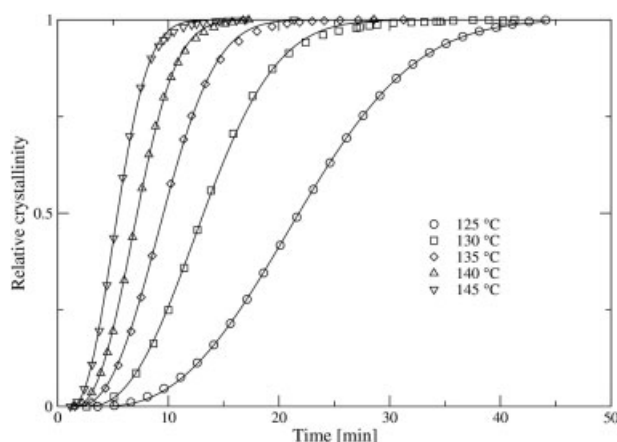


Figure 4. Relative crystallinity curve of low-temperature isotherms, between 125 and 145 °C.

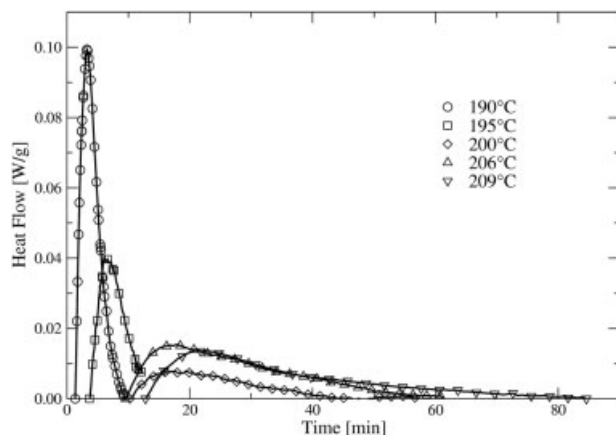


Figure 5. Heat flows versus time of high-temperature isotherms, between 190 and 209 °C.

lowers the overall crystallization rate and the polymer crystallization takes place at longer times.

A good agreement between the Avrami model (eq. 2) and the experimental data was observed, as shown in Figures 3–6. The good fitting is an indirect evidence that secondary crystallization is negligible and, as described below, the Avrami parameters can be used to analyze the crystallization mechanism of the high molecular weight PET studied in this work.

As listed in Table 1, the Avrami exponent n , which represents the nucleation mechanism and the number of growth directions, is nearly 3. Most of the data varied from a maximum of 3.2 to a minimum of 2.8 except for one testing condition (206 °C) where n was 2.2. These results are slightly higher than those reported by Lu et al.,⁴ as listed in Table 2, suggesting that the nucleation and growth mechanisms were slightly influenced by the modification of the macromolecular structure induced by the chain extension/branching reaction.

The induction time decreased with temperature in the cold crystallization range, due to the raising of the molecular mobility. On the con-

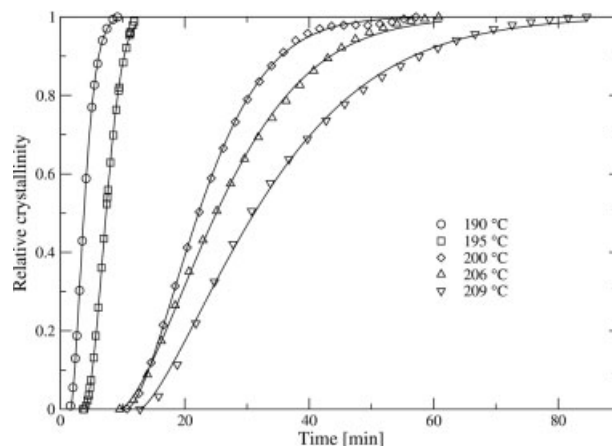


Figure 6. Relative crystallinity curve of high-temperature isotherms, between 190 and 209 °C.

trary, in melt crystallization temperature range the induction time grows because of the difficulty to nucleate a high number of stable nuclei. The low undercooling induces a weak thermodynamical instability and increases the critical radius of the nucleus. For this reason, according to experimental data, in the cold crystallization range t_0 is less sensitive to temperature respect to the melt crystallization range.

To compare the crystallization rates of MPET with the bottle grade PET from ref.⁴, the crystallization half-time $t_{1/2}$ (the time at which the relative crystallinity reaches the 50%), instead of the crystal growth rate G according to ref.³⁶, was used to evaluate the Hoffman-Lauritzen thermodynamical parameters U and K_g (eq 4):

$$t_{1/2}^{-1} = t_{1/2,0}^{-1} \exp[-U/R(T-T_C)] \exp[-K_g/fT_C \Delta T], \quad (4)$$

where $t_{1/2,0}$ is a preexponential factor, T_C is the crystallization temperature, ΔT (melt undercooling) is the difference between the thermodynamic melt temperature T_m^0 and the actual temperature T , f is a corrective factor equal to $2T_C/(T_C+T_m^0)$. The U parameter is the heat of activa-

Table 1. Values of Avrami Model Parameters Chain-Extended PET (MPET)

Parameter	Cold Crystallization					Melt Crystallization				
	125	130	135	140	145	190	195	200	206	209
Temperature (°C)	125	130	135	140	145	190	195	200	206	209
t_0 (min)	3.6	2.6	1.6	1.4	1.2	1.6	3.8	10.7	9.5	12.8
n	2.8	2.8	3.0	3.2	3.0	2.9	2.8	2.9	2.2	3.1
$K \cdot 10^3$ (min ⁻ⁿ)	0.12	0.46	0.77	1.10	4.00	12.00	1.90	0.12	0.049	0.029
$t_{1/2}$ (min)	22.1	13.2	9.55	7.3	5.4	3.75	7.2	21	25	28

Table 2. Values of Avrami Model Parameters, Bottle Grade PET (from ref. 4)

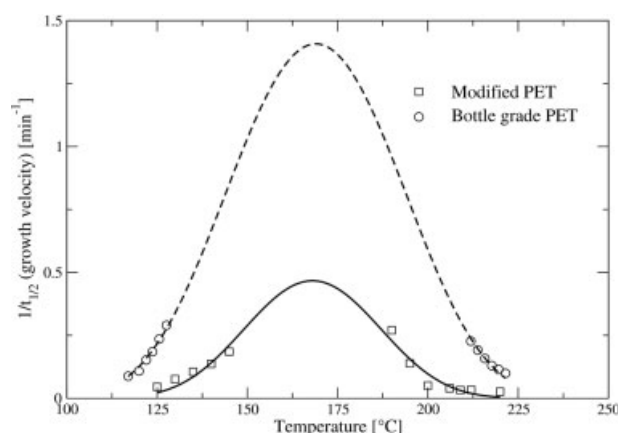
Parameter	Cold Crystallization					Melt Crystallization						
	117.9	119.8	121.7	123.6	125.5	127.5	211.8	213.7	215.7	217.6	219.5	221.4
Temperature (°C)	117.9	119.8	121.7	123.6	125.5	127.5	211.8	213.7	215.7	217.6	219.5	221.4
n	2.6	2.5	2.6	2.7	2.6	2.5	2.7	2.7	2.7	2.5	2.5	2.4
$K * 10^3$ (min ⁻ⁿ)	1.24	2.66	5.19	7.24	18.60	68.00	12.60	7.99	4.75	4.20	3.49	2.71
$t_{1/2}$ (min)	11.4	9.26	6.57	5.42	4.25	3.45	4.41	5.22	6.33	7.71	8.72	10.1

tion of the chain diffusion, while the K_g parameter is related to the free energy of formation of a nucleus of critical size.

In Figure 7 the experimental data (square marks) and the fitting values of $1/t_{1/2}$ (solid line) versus crystallization temperature are compared to those of bottle grade PET, taken from Lu et al.⁴

The curve of the chain-extended PET exhibited a peak value that was one-third of the bottle-grade PET, confirming the lower crystallization rate of the MPET at every temperature. The energetic term U , related to the molecular mobility, was evaluated from the experimental data obtained at lower temperatures ($T = 125$ – 145 °C) while the nucleation term K_g from the data at higher temperatures ($T = 190$ – 209 °C). As reported in Table 3, the curve of the MPET is characterized by higher values of U and K_g .

The value of U shows that the diffusional motions of chains from the amorphous phase to the growing nuclei (crystalline phase) are reduced by the increased MW, MWD, and eventual presence of branched macromolecules, as also reported in ref.³⁷ The rheological behavior of chain-extended and bottle-grade PET are compared in Figure 8. The complex viscosity of the MPET is higher in the whole frequency range and does not display the typical Newtonian

**Figure 7.** Crystallization rate curves of modified (solid line) and bottle-grade (dashed line) PET.

behavior at low frequency, as observed in bottle-grade PET. This behavior can be related not only to an increase of molecular weight of PET but also to the presence of irregularities along the macromolecules that modify the dependence of complex viscosity η^* with frequency.^{39–41} The modification of rheological properties is, in fact, associated to the increase in average relaxation time and broadening of relaxation time distribution as a result of chain extension and branching, as already reported by Xanthos et al.^{1–3}

The theoretical expression of K_g can be used to make some considerations about the effect of modification of the polymer on the structural characteristics of crystals (eq. 5).

$$K_g = (4b\sigma\sigma_e T_m^0) / (\Delta H_f^0 k) \quad (5)$$

The slight increase of K_g observed in MPET can be due to several factors related to the thermodynamic properties of the crystals. The equilibrium melting point T_m^0 of MPET was evaluated by using the well known Hoffman-Weeks⁴² analysis and reported in Figure 9. The melting point of the MPET ($T_m^0 = 271$ °C) was found to be significantly lower than that of bottle grade PET⁴ ($T_m^0 = 290$ °C). For this reason, the slight increase of K_g can be attributed to the increase of the free surface energies σ and σ_e (respectively, the energy of the chain folding side and of its end) probably caused by the presence of some structural irregularities along the MPET macromolecule.

X-ray analysis showed that the crystal morphology of the MPET and bottle-grade PET were characterized by the same diffraction peaks (Fig. 10), suggesting that the chemical modification did not affect the packing distance in crystals.

Table 3. Energetic Barrier Values

Polymer Type	U J mol ⁻¹	K_g °C ²
Chain extended PET	8'589	4.75 10 ⁵
Bottle grade PET	5'669	4.39 10 ⁵

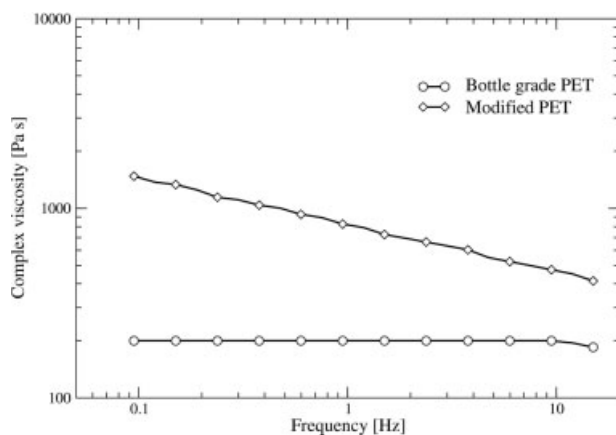


Figure 8. Rheological behavior of different types of PET.

The heat of fusion ΔH_f is therefore expected to be the same in both MPET and bottle-grade PET.

These variations can be justified if branching occurred during chemical modifications with PMDA, that, influencing the perfection degree of crystals leads to crystalline phase structure alterations. In this way the growing nucleus, to form a stable aggregate, meets a higher energy barrier to overcome in the chain extended PET respect to that of the standard polymer.

The effect of broadening of the molecular weight on crystallization of foaming grade PET has not been studied in detail so far; therefore, it is difficult to establish clear correlations between the MWD and the crystallization behavior of the PET studied in this work. On the contrary, the effect of polydispersity on crystallization kinetics was recently investigated on HDPE.⁴³ The authors found that the isothermal crystallization

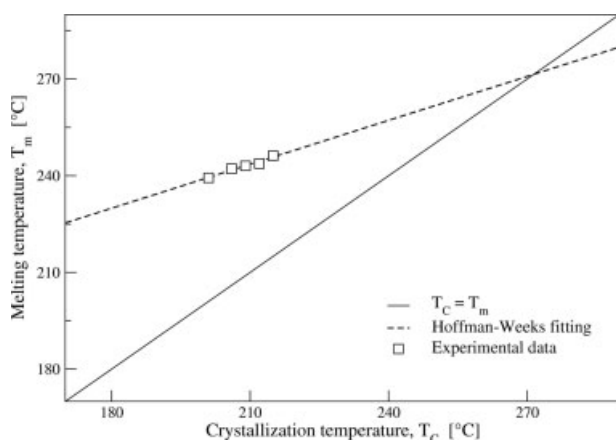


Figure 9. Hoffman-Weeks regression of chain-extended PET data for T_{m0} evaluation.

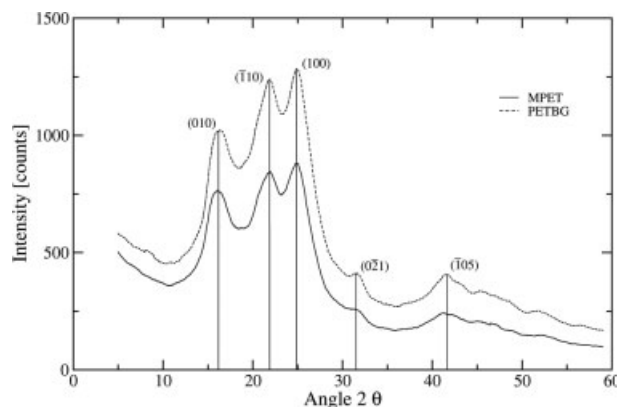


Figure 10. X-ray pattern of bottle-grade PET (PETBG) and chain-extended PET (MPET).

behavior of materials with broad MWD followed same trends as crystallization of materials with narrow MWD, even if some small differences caused by the broad MWD were observed. Due to the lack of literature data on PET more work on this issue should be done to clarify the role of the MWD versus branching on the crystallization behavior of these foaming-grade PET.

CONCLUSIONS

The crystallization behavior of a commercial chain-extended PET with high molecular weight was evaluated and compared to that of bottle-grade PET. The commercial chain-extended PET showed slower crystallization kinetics in the temperature ranges analyzed. The energetic barriers to nucleation (K_g) and molecular mobility (U) of the chain foldings moving from the melt to the growing crystals were higher for the chain-extended PET, suggesting that the chain-extending reactions introduced some variations in the macromolecular structure, probably due to partial branching, as also suggested by other authors.^{1-3,32-35} This resulted in a lower nucleation rate in both cold and melt crystallization. More work should be done to clarify the role of the MWD versus branching on the crystallization behavior of foaming grade PET.

REFERENCES AND NOTES

1. Dhavalikar, R.; Yamaguchi, M.; Xanthos, M. J. *Polym Sci Part A: Polym Chem* 2003, 41, 958–969.
2. Xanthos, M.; Yilmazer, U.; Dey, S. K.; Quintans, J. *Polym Eng Sci* 2000, 40, 554–566.

3. Xanthos, M.; Wan, C.; Dhavalikar, R.; Karayannidis, G. P.; Bikiaris, D. N. *Polym Int* 2004, 53, 1161–1168.
4. Lu, X. F.; Hay, J. N. *Polymer* 2001, 42, 9423–9431.
5. Wang, Z. G.; Hsiao, B. S.; Sauer, B. B.; Kampert, W. G. *Polymer* 1999, 40, 4615–4627.
6. Piccarolo, S.; Brucato, V.; Kieffe, Z. *Polym Eng Sci* 2000, 40, 1263–1272.
7. Ozawa, T. *Polymer* 1971, 12, 150–157.
8. Sajkiewicz, P.; Carpaneto, L.; Wasiak, A. *Polymer* 2001, 42, 5365–5370.
9. Avrami, M. *J Chem Phys* 1939, 7, 1103–1112.
10. Avrami, M. *J Chem Phys* 1940, 8, 212–224.
11. Avrami, M. *J Chem Phys* 1941, 9, 177–184.
12. Maderek, E.; Strobl, G. R. *Colloid Polym Sci* 1983, 261, 471–476.
13. Strobl, G. R.; Engelke, T.; Maderek, E.; Urban, G. *Polymer* 1983, 24, 1585–1589.
14. Sauer, B. B.; Kampert, W. G.; Neal Blanchard, E.; Threefoot, S. A.; Hsiao, B. S. *Polymer* 2000, 41, 1099–1108.
15. Elsnér, G.; Koch, M. H. J.; Bordas, J.; Zachmann, H. G. *Makromol Chem* 1981, 182, 1263–1269.
16. Santa-Cruz, C.; Stribeck, N.; Zachmann, H. G.; Balta-Calleja, F. J. *Macromolecules* 1991, 24, 5980–5990.
17. Verma, R. K.; Hsiao, B. S. *Trends Polym Sci* 1996, 9, 312–319.
18. Bassett, D. C.; Olley, R. H.; Al Raheil, I. A. M. *Polymer* 1988, 29, 1745–1754.
19. Hsiao, B. S.; Gardner, K. H.; Wu, D. Q.; Chu, B. *Polymer* 1993, 34, 3986–3995.
20. Lattimer, M. P.; Hobbs, J. K.; Hill, M. J.; Barham, P. J. *Polymer* 1992, 33, 3971–3973.
21. Verma, R. K.; Marand, H.; Hsiao, B. S. *Macromolecules* 1996, 29, 7767–7775.
22. Verma, R. K.; Kander, R. G.; Velikov, V.; Marand, H.; Chu, B.; Hsiao, B. S. *Polymer* 1996, 37, 5357–5365.
23. Wunderlich, B. *Macromolecular Physics: Crystal Nucleation, Growth, Annealing*; Academic Press: London, 1976; vol. 2.
24. Lin, C. C. *Polym Eng Sci* 1983, 23, 113–116.
25. Price, F. P. In Wunderlich, B., Ed.; *Macromolecular Physics: Crystal Nucleation, Growth, Annealing*; Academic Press: London, 1976; vol. 2.
26. Mandelkern, L. *Crystallization of Polymers*; Cambridge University Press: Cambridge, 1964; vol. 2.
27. Kim, S. P.; Kim, S. C. *Polym Eng Sci* 1991, 31, 110–115.
28. Banks, W.; Sharples, A. *J Polym Sci Part A: Gen Papers* 1964, 2, 4059–4067.
29. Tobin, M. C. *J Polym Sci: Polym Phys* 1974, 12, 399–406.
30. Tobin, M. C. *J Polym Sci: Polym Phys* 1976, 14, 2253–2257.
31. Hoffman, J. D.; Lauritzen, J. I., Jr. *J Res Natl Bour Stand A: Phys Chem* 1961, 65A, 297–336.
32. Khemani, K. C. *Annual Technical Conference*, 56th ed.; Soc Plastics Eng 1998, 2, 1934–1938.
33. Chae, H. G.; Kim, B. C.; Im, S. S.; Han, Y. K. *Polym Eng Sci* 2001, 41, 1133–1139.
34. Rhein, R. A.; Ingham, J. D. *Polymer* 1973, 14, 466–468.
35. Bratyshak, M.; Brostow, W.; Castano, V. M.; Donchak, V.; Gargai, H. *Mater Res Innovat* 2002, 6, 153–159.
36. Chan, T. W.; Isayev, A. I. *Polym Eng Sci* 1994, 34, 461–471.
37. Jayakannan, M.; Ramakrishnan, S. *J Appl Polym Sci* 1998, 74, 59–66.
38. Incarnato, L.; Scarfato, P.; Di Maio, L.; Acierno, D. *Polymer* 2000, 41, 6825–6831.
39. Wang, X. S.; Yan, D.; Tian, G. H.; Li, X. G. *Polym Eng Sci* 2001, 41, 1655–1664.
40. Rosu, R. F.; Shanks, R. A.; Bhattacharya, S. N. *Polym Int* 2000, 49, 203–208.
41. Lohse, D. J.; Milner, S. T.; Fetters, L. J.; Xenidou, M.; Hadjichristidis, N.; Mendelson, R. A.; Garcia-Franco, C. A.; Lyon, M. K. *Macromolecules* 2002, 35, 3066–3075.
42. Hoffman, J. D.; Weeks, J. *J Res Natl Bour Stand A: Phys Chem* 1962, 66A, 13–28.
43. Krumme, A.; Lehtinen, A.; Viikna, A. *Eur Polym J* 2004, 40, 359–369.